Evaluation of the End Effect Impact on the Torsion Test for Determining the Shear Modulus of a Timber Beam through a Photogrammetry Approach

Niaz Gharavi, Hexin Zhang, Yanjun Xie

Abstract—The timber beam end effect in the torsion test is evaluated using binocular stereo vision system. It is recommended by BS EN 408:2010+A1:2012 to exclude a distance of two to three times of cross-sectional thickness (b) from ends to avoid the end effect; whereas, this study indicates that this distance is not sufficiently far enough to remove this effect in slender cross-sections. The shear modulus of six timber beams with different aspect ratios is determined at the various angles and cross-sections. The result of this experiment shows that the end affected span of each specimen varies depending on their aspect ratios. It is concluded that by increasing the aspect ratio this span will increase. However, by increasing the distance from the ends to the values greater than 6b, the shear modulus trend becomes constant and end effect will be negligible. Moreover, it is concluded that end affected span is preferred to be depth-dependent rather than thickness-dependant.

Keywords—End effect, structural-size torsion test, shear properties, timber engineering, binocular stereo vision.

I. INTRODUCTION

THE end effect has a significant impact on the local twist rate, stress distribution and the fracture model of a timber beam in the torsional test. It is a common sense according to Saint-Venant's Principal [1], when testing structure samples the measuring points should be located at a distance from the supports/loads. This is due to the stress concentration at the regions close to supports/loads and since the torsion theory represents a uniform shear stress distribution along the beam; therefore, the distance which affected by end stress needs to be removed in shear properties determination. It seems that the recommendation detailed in BS EN 408 Clause 11.1.2 [2] for the torsion test has not well considered the impact of this effect, especially for the beams with high aspect ratio cross-sections. According to the aforementioned standard, the rotations should be measured within a distance of two to three times of cross-sectional thickness (b) from the supports. This specification is conditionally acceptable for the beams with low cross-sectional aspect ratios, for instance, a square section. However, the most popular cross-sections of timber beams used in construction are slenderer cross-section with an aspect ratio of 3 to 5. For these types of section, the specified setup clearly is too closed to the loading/support points which bring in unnecessary error in the rotation measurement. The torsion

test is widely recognised as a suitable method for evaluating the shear properties of timber beams as it creates a perfect pure shear status in a specimen [3]–[6], thus it is important to investigate how the end effect propagates from the ends.

The finite element analysis of stress distribution of a timber beam subjected to a torque at one end by Gupta et al. [7], indicated a distance of two times of cross-sectional depth plus grip distance needs to be excluded from both ends in order to obtain a uniform shear stress distribution. Comparing to the distance recommended by BS EN 408 [2] which is between two and three times the cross-sectional thickness, there is a significant difference for beams with slender cross-sections. To provide proper guidelines to the industry for measuring the shear properties using torsion test method, there is a need to understand the propagation of the end effect in a torsion test. The aim of this study is to investigate on the propagation of end effect in torsion test through the experimental approach using close-range photogrammetry technology.

Typically, inclinometers or modified inclinometers as indicated in the BS EN 408 [2] are used to approximate the angle of rotation for an element in a torsion test, but they are limited to record only the rotation of a specific plane at a predetermined location. It is difficult to use this type of device/design to measure the distribution of rotation on a sample during the test. Therefore, a more advanced and accurate close-range photogrammetry technology based on stereo-vision has been employed to capture the beam deformation during the test. Using the triangulation algorithm, the displacements of any point in the cameras field-of-view can be measured by with two sets of photos taken before and after the loading. One of the well-known methods of acquiring the 3-D shape coordinate of an object is Binocular Stereo Vision. Binocular Stereo Vision is a passive triangulation technique, where images taken from two different viewpoints are analysed to extract the depth map of the scene [8], [9]. This system is similar to simplified human visual perception. In this system, cameras have the same parameters (e.g. Focus length, iso setting etc.) and are mounted exactly parallel to each other. However, in reality, the stereo system setup is more complex and all the assumption made for the simplified stereo-vision system required modification. Moreover, there is some level of distortion in the acquired images regardless of the type of cameras and lenses, therefore to compensate this issue system needs to be calibrated.

N. Gharavi and H. Zhang are with the School of Engineering and Built Environment, Edinburgh Napier University, Edinburgh, EH10 5DT, UK (e-mail: n.gharavi@napier.ac.uk, j.zhang@napier.ac.uk).

Y. Xie is with College of Material Science and Engineering, Northeast Forestry University, 26 Hexing Road, Harbin, 150040, China (e-mail: yxie@nefu.edu.cn).

World Academy of Science, Engineering and Technology
International Journal of Mechanical and Mechatronics Engineering
Vol:11, No:3, 2017

TABLE I
MATERIAL INFORMATION

Nominal Dimensions			QTY	A.R.	M.C.	Specie
b [mm]	h [mm]	L [m]			[%]	
95	95	1.9	2	1	12.8	RP
45	95	1.9	2	2.11	10.4	RP
75	225	4.3	2	3	11.2	WW
45	170	3.4	2	3.78	10.4	WW
45	195	3.9	2	4.33	12	RP
45	220	4.3	2	4.89	12.5	WW

A.R.= Aspect Ratio (h/b); M.C.= Moisture Content; RP= Redwood Pine; WW= White Wood (Spruce)

II. MATERIALS AND METHODS

A. Materials

Six rectangular structural-size, kiln dried and sawn timber beams with testing length of at least 19 times of the largest cross-sectional dimension and various aspect ratios (h/b, where h = depth and b = thickness of the specimen) were obtained. Based on BS EN 408 [2], all the tests were conducted on pieces, which conditioned at the standard environment of $20 \pm 2°C$ and $65 \pm 5\%$ relative humidity for about four weeks before testing began to allow them to come to equilibrium. Moreover, the moisture content of the samples was measured in accordance with EN 13183-1 [10], which can be found in Table I.

B. Stereo Vision System

Humans and most animals' visual perception are through the highly sophisticated 3D vision system. The binocular stereo vision system is able to compute disparity, distance and 3D coordinates of objects by the simulation of human eyes. Two cameras simultaneously capture the images of an object from different positions and angles [11]. The basic principle behind binocular stereo vision is given in Fig. 1. In the figure, assume $oxyz$ is the camera coordinate systems (CCS), XOY is left and right image coordinate system and f is the effective focal length, which is the distance between camera coordinate system (lenses) and image coordinate system (image sensor within the camera). Parameters that relate to left and right images are subscripted by l and r, respectively. For convenience, the world coordinate system (WCS) is made of left camera coordinate system ($oxyz = o_l x_l y_l z_l$).

The spatial positional relationship between the world coordinate system and right camera coordinate system can be obtained as:

$$\begin{bmatrix} x_r \\ y_r \\ z_r \end{bmatrix} = M \begin{bmatrix} x \\ y \\ z \\ 1 \end{bmatrix} = \begin{bmatrix} r_{11} & r_{12} & r_{13} & t_x \\ r_{21} & r_{22} & r_{23} & t_y \\ r_{31} & r_{32} & r_{33} & t_z \end{bmatrix} \begin{bmatrix} x \\ y \\ z \\ 1 \end{bmatrix} \quad (1)$$

where $M = [R|T]$, $[R]$ expresses the rotation matrix and $[T]$ is translation transform vector between world coordinate system ($oxyz$) and right camera coordinate system ($o_r x_r y_r z_r$);

$$R = \begin{bmatrix} r_{11} & r_{12} & r_{13} \\ r_{21} & r_{22} & r_{23} \\ r_{31} & r_{32} & r_{33} \end{bmatrix}, T = \begin{bmatrix} t_x \\ t_y \\ t_z \end{bmatrix} \quad (2)$$
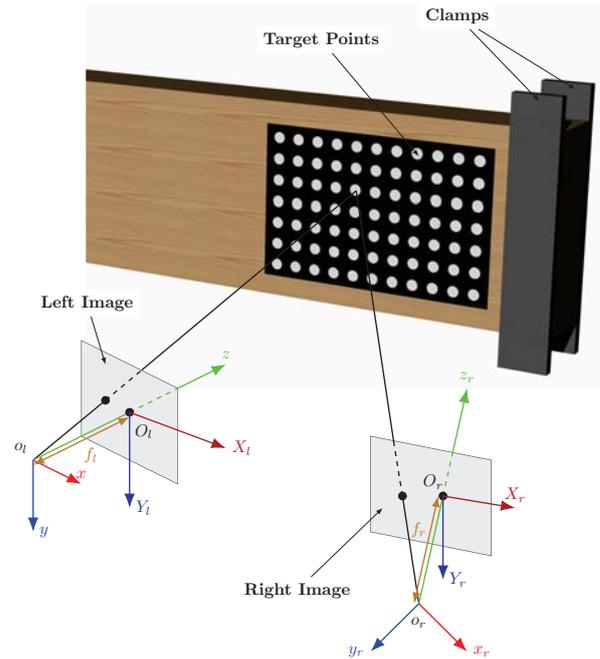

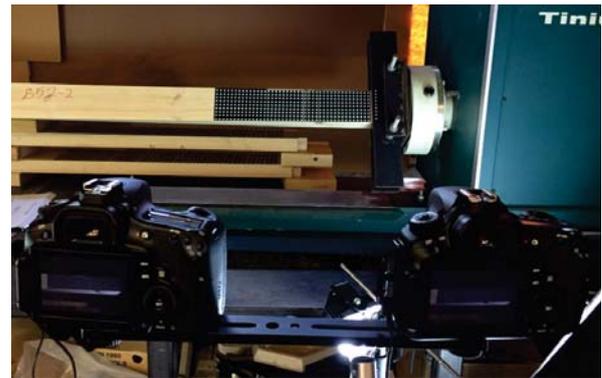Fig. 1 Target points reconstruction of binocular stereo vision

Fig. 2 Target points reconstruction of binocular stereo vision

According to the pinhole imaging theory the following expression can be made,

$$s_l \begin{bmatrix} X_l \\ Y_l \\ 1 \end{bmatrix} = \begin{bmatrix} f_l & 0 & 0 \\ 0 & f_l & 0 \\ 0 & 0 & 1 \end{bmatrix} \begin{bmatrix} x \\ y \\ z \end{bmatrix}, \quad s_r \begin{bmatrix} X_r \\ Y_r \\ 1 \end{bmatrix} = \begin{bmatrix} f_l & 0 & 0 \\ 0 & f_l & 0 \\ 0 & 0 & 1 \end{bmatrix} \begin{bmatrix} x_r \\ y_r \\ z_r \end{bmatrix} \quad (3)$$

For the spatial point in the WCS, the corresponding coordinates in the left and right image can be obtained as;

$$\rho \begin{bmatrix} X_r \\ Y_r \\ 1 \end{bmatrix} = \begin{bmatrix} f_r r_{11} & f_r r_{12} & f_r r_{13} & f_r t_x \\ f_r r_{21} & f_r r_{22} & f_r r_{23} & f_r t_y \\ r_{31} & r_{32} & r_{33} & t_z \end{bmatrix} \begin{bmatrix} z\frac{Y_l}{f_l} \\ z\frac{Y_l}{f_l} \\ z \\ 1 \end{bmatrix} \quad (4)$$

and finally, 3D coordinate of the object can be obtained as;

$$\begin{cases} x = z\frac{X_l}{f_l} \\ y = z\frac{Y_l}{f_l} \\ z = \frac{f_l(f_r t_x - X_r t_z)}{X_r(r_{31}X_l + r_{32}Y_l + r_{33}f_l) - f_l(r_{11}X_l + r_{12}Y_l + r_{13}f_l)} \\ \quad = \frac{f_l(f_r t_y - Y_r t_z)}{Y_r(r_{31}X_l + r_{32}Y_l + r_{33}f_l) - f_l(r_{21}X_l + r_{22}Y_l + r_{23}f_l)} \end{cases} \quad (5)$$

World Academy of Science, Engineering and Technology
International Journal of Mechanical and Mechatronics Engineering
Vol:11, No:3, 2017

Fig. 3 Selected round regions

In (5), if each camera's focal length f_l, f_r and the coordinates of the spatial point in both left and right images are known, the three-dimensional coordinates of the point in WCS can be obtained. Rotation matrix and translation transform vector can also be obtained by calibration.

When stereo vision system is employed to determine 3D coordinates, camera calibration is the way of determining the relationship between camera lens and image plane and also between the cameras and the calibration rig [9]. The overall performance of the computer vision system strongly depends on the accuracy of the camera calibration. The camera calibration process followed the instruction given by MVTech Halcon developer manual. In this experiment, 100 mm×100 mm calibration plate, which is purchased from MVTec Software GmbH distributor, has been used. therefore the calibration process conducted with acceptable accuracy. First step of processing the images is to select the pixels from the input image whose gray values are between appropriate minimum and maximum values, to differentiate the target points from the rest of image. The output of previous step is a regions which contains all the target points and the areas with the same gray values in the range. From the selected regions, circular regions with 80% roundness and specific diameters range, have been chosen and the centre of the selected regions determined as the target points coordinates (Fig. 3).

C. Torsion Test

The torsion test procedure followed BS EN 408 [2] using a 1 kN.m Tinius Olsen torsion test machine. The test piece mounted securely edgewise with vice-like grip at the support and the centre of specimen ends were in a line to allow it to rotate about its longitudinal axis while being subjected to torsion test. In order to create a condensed grid of data points (Fig. 2), a multiple black and white dot system was created, using a 10 mm horizontal and vertical spacing. The cameras selected for this project were four Canon EOS 550Ds, which are an 18.0 megapixel digital single-lens reflex camera, and equipped with 50 mm Canon EF f/1.8 II fixed focal lenses.

After obtaining all required calibration and test photographs, a reiterating code was developed for the Halcon 11 stereo vision software. The area command could be utilised to seek each target within the target template. To eliminate the machine and human errors, the first applied torque corresponding to a 4° rotation was considered as the zero point. All subsequent coordinates and forces were adjusted

accordingly. And finally, the shear modulus of each specimen is determined by the equation given in the standard under the assumption of Saint Venant's torsion theory;

$$k_{tor} = \frac{T}{\phi_i} \qquad \rightarrow \qquad G_{tor} = \frac{k_{tor}}{\eta h b^3} l_1 \qquad (6)$$

where: k_{tor} is torque stiffness, ϕ_i is rotation at each cross section (i), T is applied torque, G_{tor} is shear modulus in torsion test and l_1, η, h and b are free testing length, shape factor which is given in [2], cross-sectional height and thickness of beam, respectively.

III. RESULTS AND DISCUSSION

Figs. 4 (a) and (b) illustrate the mean shear modulus trend of each specimen against the distance of each relative rotation measured cross-sections from the specimen ends. The bottom and top x-axis in the figures show the considered cross-section's distance from ends in correlation with the thickness and depth, respectively. The shear modulus of each specimen at each cross-section determined according to the BS EN 408 [2] recommendations. Each graph is divided into two segments visually, segment one represents the end affected span and segment two represents the shear span, where the shear stress distribution is uniform. Variation of shear modulus determined at cross-sections within the segment two is significantly lower (More than 70%) than that in segment one. This is due to uniform distribution of shear stress along the beam, which led us to have a constant shear modulus. AR=1 has a considerably high coefficient of variation ($\approx 30\%$), and this is due to the beam's compress at clamps because of applying a high amount of load while having not sufficient grip resistance.

The results of this experiment revealed that two to three times of thickness, which noted in the BS EN 408 [2], in order to exclude the end clamp effect is not far enough to avoid this caveat in slender cross-sections. End affected span is directly proportional to the aspect ratio (to be exact, thickness), where for the slender cross-sections (higher aspect ratios) this span in longer and the same correlation applies with the lower aspect ratios. According to Saint Venant's principle, the end effect becomes negligible at the distances sufficiently far removed from ends [1], likewise, the results of this study indicate that end effect nearly disappears at a distance greater than $6b$ plus grip distance regardless of the cross-sectional size. Furthermore, the finite element study by Gupta et al. [7] showed that the cross-sectional size (depth of the specimen) is not an effective factor in shear stress distribution along the beam. This experiment indicates that there is not a considerable relationship between the specimen depth and the end affected span, however, specimen thickness alters the end affected span significantly.

Gupta et al. [7] recommended excluding two times of depth $(2h)$ plus grip distance from each ends to obtain a uniform shear stress distribution. The results of this study indicate that from a distance of 1-1.5 times the depth plus grip distance shear modulus becomes almost constant. Therefore, it is experimentally and theoretically reasonable to determine the shear properties of solid timber at $2h$ plus grip distance.

World Academy of Science, Engineering and Technology
International Journal of Mechanical and Mechatronics Engineering
Vol:11, No:3, 2017

Considering the shear modulus trend graphs, thickness coefficient increases considerably by increasing the aspect ratio and reaches its longest distance of $6b$ at AR=4.33 and decreases to $4.44b$ at AR=4.89. On the contrast, changes in depth coefficient are fairly steady between $1h$ and $1.5h$. Therefore, the ASTM D198 [12] specification on end affected distance, which is $2h$, is preferable to that in BS EN 408 [2], which is between $2b$ and $3b$.
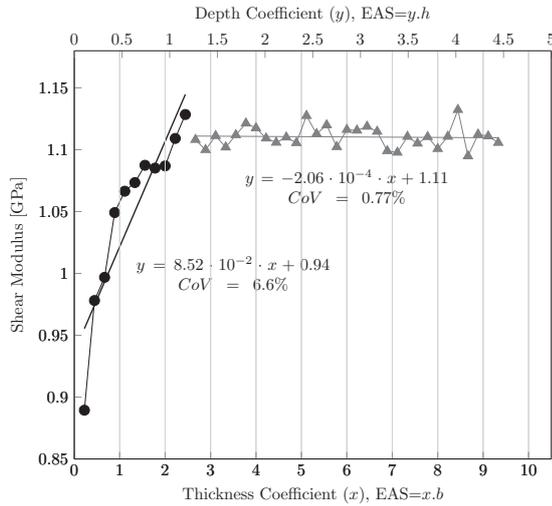
(a) AR=2.11 ; CoV=6.8% ; Red Pine
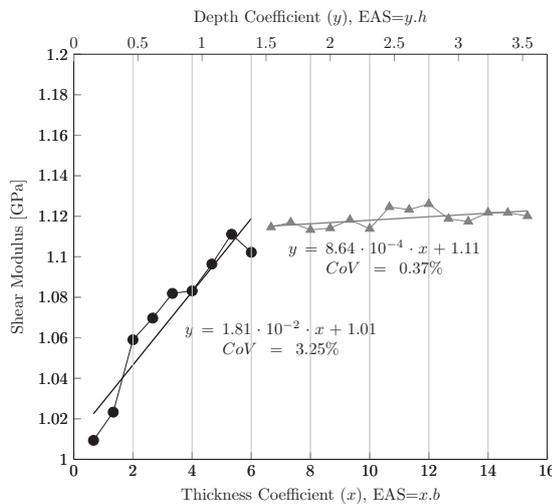
(b) AR=4.33 ; CoV=14.9% ; Red Pine

Fig. 4 Shear modulus trend

IV. CONCLUSION AND RECOMMENDATION

The following conclusion can be drawn:

1) In regards to [2], it was found that slenderness is an affecting factor in shear modulus determination. Two to three times of thickness, which is noted in the aforementioned code, is not far enough to avoid end effects in slender cross-sections. The end clamp affected distance is directly proportional to the aspect ratio, although, at a distance greater than $6b$, this effect is negligible regardless of the cross-sectional size

2) Despite, there is no literature supports the [12], [2] specifications in end affected distance, according to this study, recommendation by [12] for this distance is preferable to that in [2]. The results of this experiment revealed that, end affected distance is thickness-dependant while it is independent of depth, therefore, locating this distance in a coefficient of depth is recommended

3) The stereo vision system has the capacity to be utilized in the structural-size tests to measure the displacement and rotation in high accuracy

It is highly recommended to undertake further studies on end clamp effect and its influence on determination of shear properties of timbers products in the torsion test. Employing a high speed and high-resolution cameras would increase the accuracy of the measurements and provide continuous recording.

REFERENCES

[1] A. P. Boresi and R. J. Schmidt, *Advanced Mechanics of Materials*. John Wiley and sons, 2003.
[2] BS EN 408:2010+A1:2012, "British Standard: Timber structures Structural timber and glued laminated timber Determination of some physical and mechanical properties," *BSI Standards Publication*, 2012.
[3] L. A. Soltis and D. R. Rammer, "Shear Strength of Unchecked Glued-Laminated Beams," *Forest Product Journal*, vol. 44, pp. 51–57, 1994.
[4] R. Gupta, L. R. Heck, and T. H. Miller, "Experimental Evaluation of the Torsion Test for Determining Shear Strength of Structural Lumber," *Journal of Testing and Evaluation*, vol. 30, no. 4, p. 283, 2002.
[5] A. M. Khokhar, H. Zhang, D. Ridley-Ellis, and J. Moore, "Determining the Shear Modulus of Sitka Spruce from Torsion Tests." in *Proceedings of the 10th World Conference on Timber Engineering*, 2008.
[6] R. Gupta and T. Siller, "Shear strength of structural composite lumber using torsion tests," vol. 33, no. 2, pp. 110–117, 2005.
[7] R. Gupta, L. R. Heck, and T. H. Miller, "Finite-Element Analysis of the Stress Distribution in a Torsion Test of Full-Size, Structural Lumber," *Journal of Testing and Evaluation*, vol. 30, no. 4, p. 291, 2002.
[8] Z. Peng and N. Guo-Qiang, "Simultaneous Perimeter Measurement for 3D Object with a Binocular Stereo Vision Measurement System," *Optics and Lasers in Engineering*, vol. 48, no. 4, pp. 505–511, 2010.
[9] Christian Wohler, *3D Computer Vision, Efficient Methods and Applications*, 2nd ed. Springer, 2013.
[10] BS EN 13183-1:2002, "British Standard: Moisture content of a piece of sawn timber. Determination by oven dry method," *BSI Standards Publication*, no. December, 2007.
[11] Y. Li, P. Chen, M. Zhang, Y. Li, Á. P. Chen, and M. Zhang, "The Vehicle Distance Measurement System Based on Binocular Stereo Vision," *Lecture Notes in Electrical Engineering*, vol. 378, 2016.
[12] ASTM-D198, "Standard Test Methods of Static Tests of Lumber in Structural Sizes," *ASTM International*, pp. 1–27, 2014.